Semi-Transparent, Chiral Organic Photodiodes with Incident Direction-Dependent Selectivity for Circularly Polarized Light

ADVANCED MATERIALS
www.advmat.de

Semi-Transparent, Chiral Organic Photodiodes with Incident Direction-Dependent Selectivity for Circularly Polarized Light

Lixuan Liu, Zhixiang Wei, and Stefan C. J. Meskers**

Detection of the circular polarization of light is possible using chiral semiconductors, yet the mechanisms remain poorly understood. Semi-transparent chiral photodiodes allow for a simple experiment to investigate the basis of their selectivity: changing the side from which the diode is illuminated. A reversal of circular selectivity is observed in photocurrent generation when changing the direction of illumination on organic, bulk-heterojunction cells. The change in selectivity can be explained by a space-charge limitation on the collection of photocarriers in combination with preferential absorption of one of the circular polarizations of near-infrared light by the chiral non-fullerene acceptor. The space-charge limitation is supported by detailed measurements of frequency and intensity dependence of *dc* and *ac* photocurrents.

1. Introduction

The polarization of light carries information. The circular polarization of light is of vital importance in quantum communication, remote sensing, drug screening, and 3D display.[1–5] Chiral organic π-conjugated molecules have emerged as fascinating semiconducting materials that may be used to generate and detect light of one particular circular polarization.[6–10] Especially, non-fullerene acceptors with excellent optical and electronic properties are considered as promising candidates for developing novel chiral functional materials.[11–19] The inherent chiroptical properties of chiral organic materials can help to simplify the design of the optical devices by eliminating the need for separate polarizers and retarders.

The mechanistic understanding of the selective detection of circularly polarized light (CPL) by chiral semiconductors is still incomplete. Various mechanisms have been proposed, including selective photogeneration of electrons or holes,[20] generation of spin-polarized carriers combined with spin-dependent transport and collection,[21–23] the circular photogalvanic effect,[24–27] and differential absorption of left- and right-circularly polarized light (L- and R-CPL).[28–30] A key performance parameter in the detection of CPL is the photocurrent dissymmetry factor $g = 2(I_L - I_R)/(I_L + I_R)$, where I_L and I_R denote the photocurrent generated under illumination with L and R-CPL of exactly equal intensity. This degree of CPL selectivity in photoresponse may be compared to the corresponding dissymmetry factor for the selective absorption of light ($g_{abs} = 2(\alpha_L - \alpha_R)/(\alpha_L + \alpha_R)$ with α the absorption coefficient) by the chiral semiconductor. A number of studies reported g and g_{abs} having the same sign.[28–32] Yet, perhaps counterintuitively, opposite signs for g and g_{abs} were found for some materials.[33–36] It was also found that g can change sign depending on the thickness of the active layer.[33]

Herein, we report on the circular selective photoresponse of semi-transparent bulk-heterojunction (BHJ) organic photodiodes in the near-infrared range.[37,38] The BHJ comprises an enantiomerically pure non-fullerene acceptor and an achiral π-conjugated polymer (see **Figure 1**). The use of semi-transparent contacts allows us to measure the photoresponse for two opposite directions of illumination of the same cell. We find opposite signs for the short circuit photocurrent dissymmetry factor (g_{sc}, i.e., g at zero bias) under these two illumination geometries. Moreover, the dissymmetry ratios are found to vary in magnitude depending on the intensity of the illumination. These findings can be qualitatively explained by a device model involving circular selective absorption of light by the chiral material in combination with carrier extraction from only a narrow active zone in the active material. The results suggest that chiroptical properties in combination with charge transport characteristics determine which handedness of light is preferentially detected by organic photodiode detectors.

L. Liu, Z. Wei
CAS Key Laboratory of Nanosystem and Hierarchical Fabrication
National Center for Nanoscience and Technology
Beijing 100190, China
E-mail: weizx@nanoctr.cn

L. Liu, Z. Wei
School of Future Technology
University of Chinese Academy of Sciences (UCAS)
Beijing 100049, China

L. Liu, S. C. J. Meskers
Molecular Materials and Nanosystems
Institute for Complex Molecular Systems
Eindhoven University of Technology
P. O. box 513, Eindhoven, NL 5600MB, The Netherlands
E-mail: s.c.j.meskers@tue.nl

The ORCID identification number(s) for the author(s) of this article can be found under https://doi.org/10.1002/adma.202209730.

DOI: 10.1002/adma.202209730

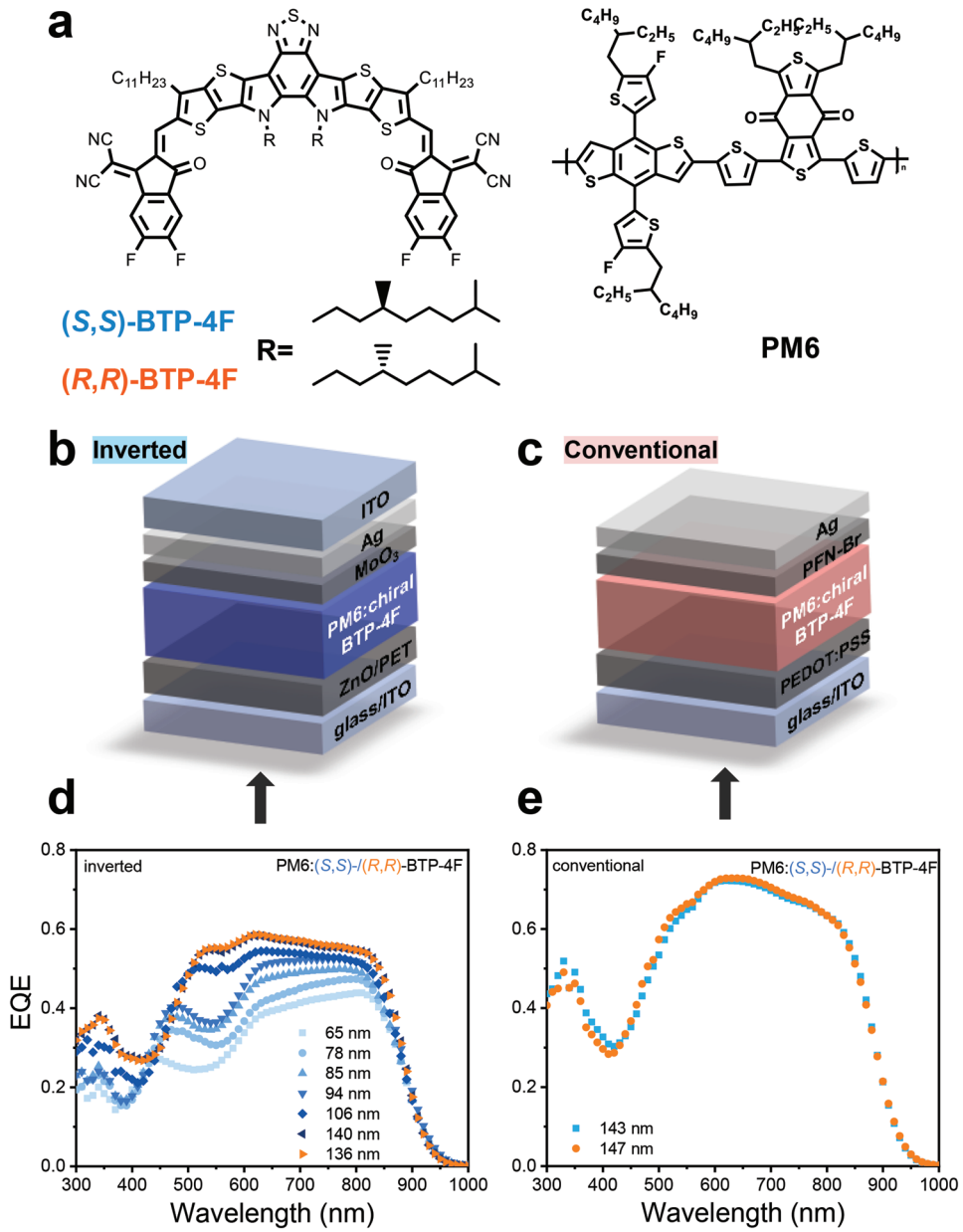

Figure 1. a) Chemical structure of the chiral acceptor and achiral polymer donor used in the bulk heterojunction. b,c) Architecture of the semi-transparent, bulk-heterojunction diodes. d,e) External quantum efficiencies of the bulk-heterojunction diodes with inverted and conventional architecture made with enantiomerically pure (*S*,*S*)- or (*R*,*R*)-BTP-4F acceptor under low light level illumination. Diodes of inverted structures with different thicknesses of PM6:(*S*,*S*)-BTP-4F were studied.

2. Results and Discussion

2.1. Semi-Transparent Bulk-Heterojunction Diodes

Bulk-heterojunction diodes involving a chiral acceptor based on the thienothienopyrrolo-thienothienoindole (BTP) core functionalized with enantiopure, 3,7-dimethyloctyl side chains, and achiral PM6 polymer donor were studied (Figure 1). For details on synthetic procedures, see the Experimental Section in Supporting Information. Matched energy levels and complementary absorption for chiral acceptors and polymer donors enable efficient exciton generation and charge separation (Figures S1–S3, Supporting Information). A donor:acceptor blend ratio of 1:9 in weight was chosen as a compromise between a high selective absorption of circularly polarized light with high acceptor loading and high quantum efficiency for photocurrent generation with balanced donor–acceptor content.[39,40] External quantum efficiencies (EQE) for photocarrier collection under illumination with low intensity, near-infrared light at short circuit conditions as high as 0.5 and 0.6 could be achieved for diodes with respectively inverted and conventional architecture, resulting in a high responsivity of 0.35 and 0.40 A W^{-1} (see Figure 1; Figure S4, Supporting Information). Additional photovoltaic properties are listed in Tables S1 and S2 (Supporting

Information). The most important figure of merit of semi-transparent diodes, average visible transmittance, evaluated from their transmittance spectra varied from 24% to 10% with the thickness increasing from 65 to 140 nm (Figure S5 and Table S3, Supporting Information). Diodes containing only acceptors generate a low short-circuit photocurrent with an EQE that is 20 times lower compared to the 1:9 D:A bulk heterojunction. Hence, we conclude that charge carriers in the 1:9 heterojunction are predominantly generated via exciton dissociation at the D:A interface.

For the diodes shown in **Figure 2**, we have determined the dissymmetry factor for short circuit photocurrent under L and R-CPL, $g_{sc} = 2(I_{sc}^{L} - I_{sc}^{R})/(I_{sc}^{L} + I_{sc}^{R})$. In these measurements, we used the light of 830 nm wavelength from a laser diode that was modulated between L and R circular polarization using a photoelastic modulator operating at 50 kHz. For each of the four different cell types, we observe that the sign of g_{sc} inverts when we change the direction of the incoming light from bottom to top. Reassuringly, g_{sc} values for diodes with acceptors of opposite absolute stereochemistry are similar in magnitude but opposite in sign for both architectures. Furthermore, we find that the absolute magnitude of g_{sc} increases when raising the intensity of the incoming light from 3.6 to 40 and to 60 mW cm^{-2}.

Further experimental support for an intensity dependence of g_{sc} is shown in **Figure 3**. This intensity dependence proves to be most pronounced in diodes with a thick BHJ layer (140 nm, see Figure 3a; Figure S6, Supporting Information). The g_{sc} increases continuously with increasing photon flux, as observed for both enantiomers of the chiral acceptor (Figure 3b; Figure S7, Supporting Information).

2.2. Space-Charge Limitation on Carrier Collection

In order to better understand the response of these diodes with highly imbalanced donor:acceptor ratio,[41–46] we have characterized the photocurrents of inverted PM6:(*S*,*S*)-BTP-4F diodes under illumination from the bottom side in detail (Figure S8, Supporting Information). Because of the skewed donor:acceptor ratio, one could expect an imbalance in the mobilities of positive and negative charge carriers that may cause a limitation in the collection of the slowest carrier due to the built-up of space-charge.[41–45] Charge carrier mobilities in diodes with different D:A ratios were determined from space-charge limited conduction (SCLC) measurement using single-carrier devices. With the decrease of PM6 content, the hole mobility also decreases. The electron and hole mobilities were calculated to be 20.6×10^{-4} and 0.63×10^{-4} cm^2 V^{-1} s^{-1} for the 1:9 blends. (Figure S9 and Table S4, Supporting Information). The μ_e is almost 33 times higher than the μ_h, fulfilling the requirement of strongly unbalanced transport for a space-charge limitation (SCL) on current collection. We indeed find evidence for such space-charge limited photocurrents, see **Figure 4**.

Following Mihailetchi et al.,[41] we first looked into how the photocurrent density $J_{ph} = J - J_{dark}$ varies as a function of the effective applied bias $V_{eff} = V_0 - V$, with V_0 the compensation voltage at which $J_{ph} = 0$, see Figure 4a . We find a square-root dependence of J_{ph} on the V_{eff} as indicated by the inclined red lines. The square-root trend is more obvious at higher light intensity. However, for the balanced D:A blends(1:1.2) no such square-root dependent region is observed (Figure S10, Supporting Information). Such a square-root dependence indicates either space-charge limited or recombination-limited photocurrent.[41,47]

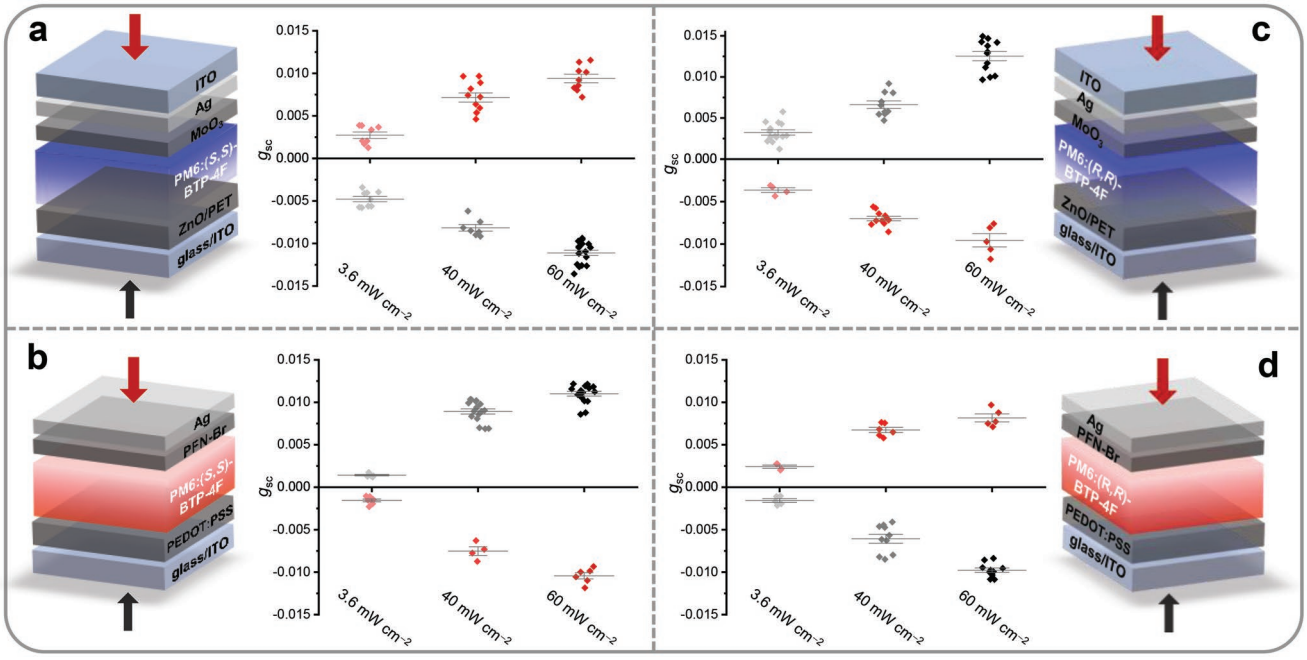

Figure 2. Dissymmetry factor for short-circuit photocurrent g_{sc} under illumination with L- and R-CPL of 830 nm wavelength with different intensities a) inverted PM6:(*S*,*S*)- BTP-4F diode, $d = 140$ nm, b) conventional PM6:(*S*,*S*)- BTP-4F diode, $d = 143$ nm c) inverted PM6:(*R*,*R*)- BTP-4F diode, $d = 136$ nm, d) conventional PM6:(*R*,*R*)-BTP-4F diode, $d = 147$ nm. The black symbols refer to illumination via the bottom contact through the glass support, the red symbols to illumination from the top side. Error bars represent the standard error of the mean.

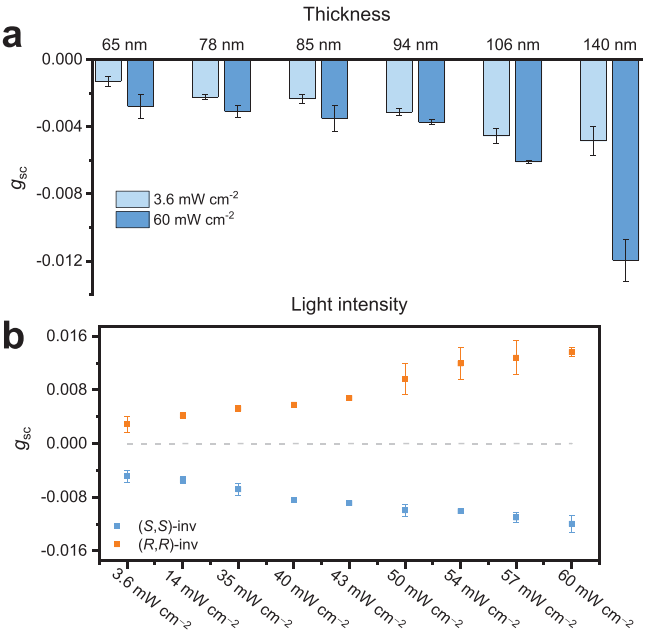

Figure 3. The dependences of g_{sc} on the thickness of the bulk heterojunction layer and light intensity for inverted diodes illuminated via the bottom contact. a) Cells with PM6:(*S*,*S*)-BTP-4F. b) Cells with 140 nm thick BHJ layer with either (*S*,*S*)- or (*R*,*R*)-BTP-4F acceptor. Error bars represent the standard error of the mean ($n = 10$).

The space-charge limited regime can be distinguished from the recombination-limited case based on the light intensity dependence of the photocurrent. If the photocurrent is SCL, it should follow:[41]

$$J_{ph} = q\left(\frac{9\varepsilon_0\varepsilon_r\mu_h}{8q}\right)^{1/4} G^{3/4}V^{1/2} \quad (1)$$

where q is the elementary charge, G is the charge carrier generation rate, $\varepsilon_0\varepsilon_r$ is the dielectric permittivity, and μ_h is the mobility of the carrier with the longest lifetime, here the hole.

In Figure 4b, the variation J_{ph} with light intensity is shown for two different effective bias voltages, one in the square-root regime and the other in the saturation region. At $V_{eff} = 0.4$ V in the square-root region, we find $J_{ph} \propto I^{\alpha}$ with $\alpha = 0.78$, while for bias in the saturation regime ($V_{eff} = 2.5$ V) a power $\alpha = 1.04$ is obtained. The proportionality of J_{ph} with light intensity to the power 3/4 at low effective bias is consistent with Equation (1), indicating a space-charge limitation on the current collection for small effective voltages. For the recombination limited case, a linear dependence ($\alpha = 1$) is expected[41] at variance with the experiments at $V_{eff} = 0.4$ V. In addition, the variation of the saturation voltage (V_{sat}) at which J_{ph} switches from the square-root to the saturation regime, also supports a space-charge limitation. We find $V_{sat} \propto I^{\alpha}$ with $\alpha = 0.51$ from the double logarithmic plot (Figure 4c). In contrast, V_{sat} is expected to be independent of light intensity in the recombination-limited case.

Further information on the width L of the space charge can be obtained from *ac* photo-capacitance measurements near open-circuit conditions.[48,49] For the case of space-charge limited photocurrent collection one predicts:

$$C_p = \frac{\varepsilon_0\varepsilon_r A}{L} \quad (2)$$

With C_p the equivalent parallel capacitance and A the device area and L the width of the space charge zone. Note that here L varies with light intensity and bias voltage. Based on Equation (2), an experimental estimate of L can be obtained from $L = d\ C_0/C_p$ with C_0 the equivalent parallel capacitance in dark and d the total thickness of the bulk heterojunction layer.

First, we check the validity of the space-charge limitation model for the ac-admittance. The equivalent parallel conductance (G_p) and capacitance (C_p) were recorded as a function of the frequency and illumination intensity by applying a small *ac* oscillating bias voltage of 50 mV and a *dc* bias voltage equal to the V_{oc} at the particular light intensity (Figure 4d,e). Expression for G_p and C_p for the case of space-charge limited photocurrent are:

$$G_p = qA\left(\frac{9\varepsilon_0\varepsilon_r\mu_h}{8q}\right)^{1/4} G^{3/4}V^{-1/2} \quad (3)$$

$$C_p = (\varepsilon_0\varepsilon_r)^{3/4}\ A\left(\frac{8q}{9\mu_h}\right)^{1/4} G^{1/4}V^{-1/2} \quad (4)$$

The relaxation time τ_p is the ratio of C_p and G_p:[48]

$$\tau_p = \frac{C_p}{G_p} = \left(\frac{8\varepsilon_0\varepsilon_r}{9\mu_h q}\right)^{1/2} G^{-1/2} \quad (5)$$

The variation of relaxation time with frequency under different light intensities is shown in Figure 4f. At low-frequency (1000 Hz), G_p, C_p, and τ_p follow power law dependencies on light intensity with exponents of +0.73 ± 0.03, +0.22 ± 0.01, and −0.51 ± 0.02, respectively. These experimental values are in close agreement with the predicted exponents of +3/4, +1/4, and −1/2 for the variation of G_p, C_p, and τ_p, respectively, with generation rate, see Equations (3–5).

In summary, detailed analysis of the photocurrents supports a space-charge limitation of carrier collection at higher illumination intensities. This behavior indicates that photocarriers generated across the bulk heterojunction can only be collected efficiently out of a thin active zone adjacent to the hole collecting contact, because of the low mobility of holes compared to electrons. Thus, only a limited zone of the total BHJ layer contributes to the photocurrent.

2.3. Mechanism and Optical Modeling

The experimental evidence for only a thin zone of the total BHJ being active in carrier collection can be incorporated into a model that can qualitatively explain the sign inversion of g_{sc} with illumination direction as well as the dependence of g_{sc} on the incoming intensity. This model is represented schematically in **Figure 5**. The scheme pertains to diodes with inverted geometry and incorporating the (*S*,*S*) acceptor. In such diodes, we expect that only carriers generated in a thin zone next to the hole collecting MoO_3 contact will contribute to the

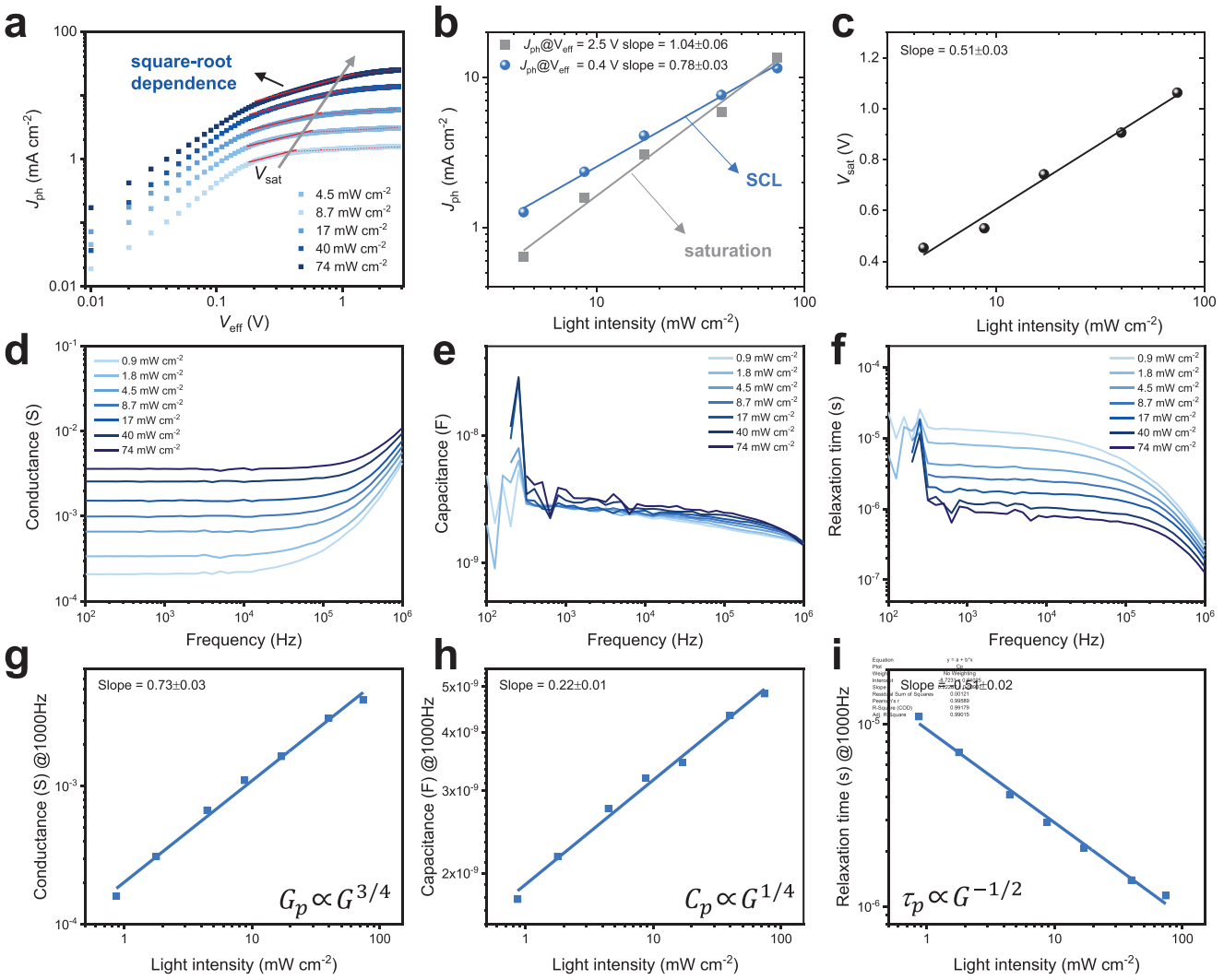

Figure 4. Opto-electronic characterization of an inverted PM6:(*S*,*S*)-BTP-4F diode with 140 nm thick active layer, illuminated from the bottom side (through the glass support) with light of 730 nm from an LED. a) Dependence of photocurrent J_{ph} on V_{eff} for different light intensities. The red solid lines shows $J_{ph} \propto V_{eff}^{1/2}$ and the red dashed lines indicate the saturation regime. b) J_{ph} at V_{eff} = 0.4 V (square-root regime) and at V_{eff} = 2.5 V (saturation regime) as a function of light intensity. c) Dependence of V_{sat} extracted from the crossover of square-root and saturation region on light intensity. d–f) The dependence of G_p, C_p, and τ_p on frequency under different light intensity of inverted PM6:(*S*,*S*)-BTP-4F diodes with a thickness of 140 nm. g–i) The dependence of G_p, C_p, and τ_p at 1000 Hz on light intensity.

photocurrent, as explained above. This active zone is indicated schematically by the filled blue rectangle in Figure 5.

If the absorption coefficient of the (*S*,*S*)-bulk heterojunction for L-CPL is higher than for R-CPL, then photons absorbed in this active zone from a light beam entering via the adjacent, hole collecting contact, will have predominantly L polarization. In contrast, for light entering via the opposite, electron collecting contact, photons absorbed in the active zone will have majority R circular polarization because most of the L polarized photons will already have been absorbed by the part of the heterojunction that is not effective in producing extractable carriers. Hence, based on this simple reasoning, one expects an inversion of the sign of g_{sc} upon changing the direction of the incoming light.

The model proposed in Figure 5 can, in a qualitative way, also account for the intensity dependence of g_{sc}. To illustrate this, we first model the absorption of photons in the active zone of PM6:(*S*,*S*)-BTP-4F diodes as a function of the width L of the active zone. First, we discuss a simplified model where the intensity $I_{L(R)}$ of L(R)-CPL in the active layer decreases exponentially as it propagates through the heterojunction layer according to $I_{L(R)}(x)/I_0 = \exp(-\alpha_{L(R)} \cdot x)$. Here, the extinction coefficients α_L and α_R are calculated from the imaginary part of the refractive index $\kappa = 0.9$ at 830 nm as determined from spectroscopic ellipsometry via $\alpha = 4\pi\kappa/\lambda_0$ and assuming $g_{abs} = 2(\alpha_L - \alpha_R)/(\alpha_L + \alpha_R) = +0.015$. The simple analytic expression for the intensity of the light then allows for straightforward numerical estimation of the number of absorbed photons in the active zone with thickness L.

Assuming then that all photons absorbed in the active zone contribute a collected carrier while all photons absorbed outside the active zone contribute none, g_{sc} can be computed directly,

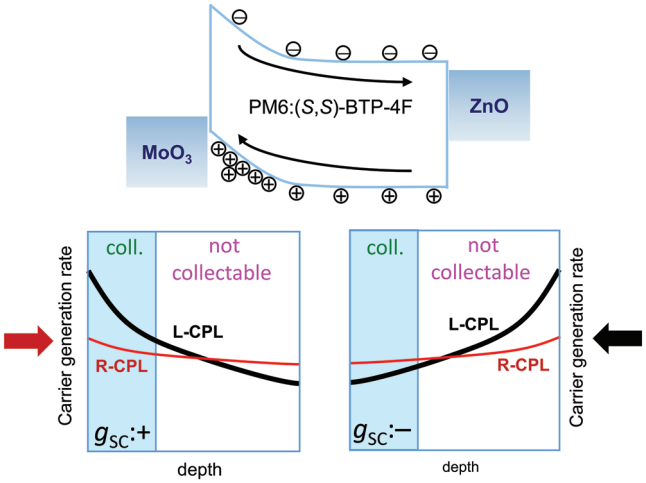

Figure 5. Model proposed for photogeneration and collection of carriers in the PM6:(*S*,*S*)BTP-4F bulk heterojunction. Carriers are generated throughout the heterojunction. Yet, due to the low mobility of holes, only those carriers generated close to the hole collecting contact (MoO_3) in the space charge zone can be harvested.[47] Illumination via the hole collecting contact results in preferential absorption of L-CPL in the active zone for carrier collection (filled blue rectangle), if the extinction coefficient for absorption of L-CPL light by the PM6:(*S*,*S*)-BTP-4F is higher than for R-CPL. Illumination of the BHJ via the electron collecting contact (ZnO) will result in a higher carrier generation rate in the active zone upon illumination with R-CPL, because most of the L-CPL has already been absorbed by part of the BHJ that is inactive in carrier collection.

see **Figure 6**. This simple model indeed predicts oppositely signed g_{sc} when reversing the direction of illumination, provided that the width of active zone L is <110 nm for a diode with a 140 nm thick BHJ layer. We note that this simplified optical modeling neglects any internal reflection of light within the diode and also any absorption in layers other than the BHJ. Detailed optical modeling using the transfer matrix method confirms the validity of these simplifications; see the half-moon symbols in Figure 6 (Supporting Information).

To compare these model predictions with experimental g_{sc} values, we first estimate the width L of the active zone in the diode from the photocapacitance measurements shown in Figure 4e following the simple relation $L = d\ (C_0/C_p)$ with d the total thickness of the BHJ layer, C_p the parallel capacitance at 10^5 Hz, and C_0 the corresponding capacitance in dark. The results are shown as blue squares in Figure 6. As can be seen, the model calculations reproduce the experimentally observed trend of increasing g_{sc} with increasing illumination in a qualitative manner. The experimental data suggest a much steeper variation of g_{sc} with the width L of the active zone than predicted via optical modeling. From this disparity, we infer that the propagation of circularly polarized light through the bulk heterojunction may be more complicated than assumed in our optical model. Local optical anisotropies in the bulk heterojunction, selective scattering, and reflection, as well as perhaps nonlocal interaction of the electromagnetic wave with the material, may need to be considered.

3. Conclusion

The semi-transparent chiral organic photodiodes developed here can be illuminated for both sides and generate photocurrent with high quantum efficiency. The sign reversal of the selectivity for L and R-CPL when changing the direction of the incoming light shows that the selectivity is not determined by a single, chirality-dependent parameter of the material, but must involve a convolution of several mechanistic steps. Here, we have argued that selectivity in the absorption of left and right polarized photons in conjunction with selectivity in the collection of photogenerated carriers depending on how close they are generated to the hole collecting contact can, in a qualitative manner, account for the sign reversal of the selectivity. Our findings suggest that further optimization of chiral organic photodetectors for detection of the circular polarization of light requires careful evaluation of the interdependence of elementary reaction steps in the detection sequence such as photon absorption, carrier generation, and carrier collection. In particular, the intensity dependence study here has shown that g can increase at the expense of a lower EQE. Improving both g and EQE may be feasible through the often neglected

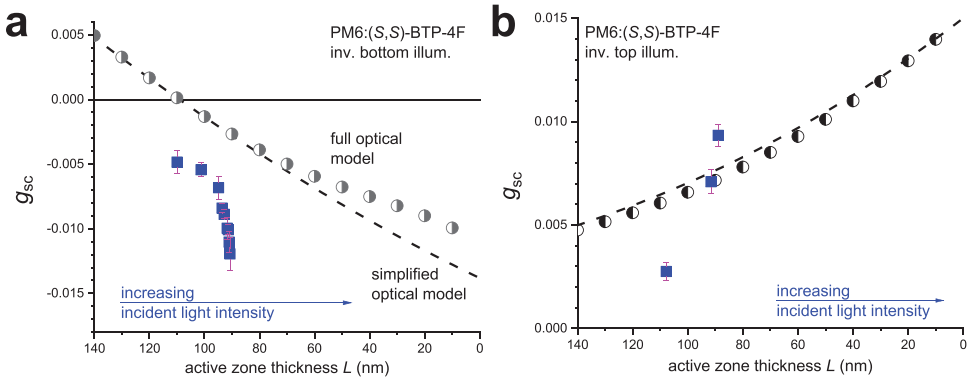

Figure 6. Short circuit photocurrent dissymmetry factor g_{sc} for PM6:(*S*,*S*)-BTP-4F diodes with inverted architecture as function of the width L of the zone active in carrier collection and carrying net space charge. The half-moon symbols show values predicted from modeling transmission, reflection, and absorption of the full stack of layers combined with a dissymmetry factor of the extinction coefficients α for L and R-CPL, $g_{abs} = +0.015$. The dashed line refers to simplified modelling where only absorption in the active layer is included. The blue squares represent experimental g_{sc} values against L estimated from measurements of the high frequency (10^5 Hz) ac capacitance under illumination at open circuit, see Figure 4e. a) illumination from the bottom side through the glass support. b) Illumination from the top side.

dependence of g_{abs} on wavevector. The very high refractive index near a narrow, intense absorption band will induce a shortening of the wavelength inside the material, allowing short-range helicity in the narrow confines of the bulk heterojunction geometry to contribute to a large circular differential response.

Supporting Information

Supporting Information is available from the Wiley Online Library or from the author.

Acknowledgements

The authors acknowledge the financial support from the Ministry of Science and Technology of China (grant no. 2021YFA1200303), the National Natural Science Foundation of China (grant nos. 21721002 and 22135001), the Strategic Priority Research Program of Chinese Academy of Sciences (no. XDB36000000), and the China Scholarship Council (202104910462). The authors thank T. van der Pol for help with device fabrication and W. van Geel for assistance with impedance measurements.

Conflict of Interest

The authors declare no conflict of interest.

Author Contributions

L.L. synthesized the acceptor molecule and fabricated devices. L.L. and S.M. characterized the cells. Z.W. planned the research and oversaw synthesis. L.L. wrote the manuscript with the help of S.M. All authors commented on it.

Data Availability Statement

The data that support the findings of this study are available from the corresponding author upon reasonable request.

Keywords

bulk-heterojunctions, circularly polarized light detection, semi-transparent photodiodes, space-charge limited photocurrents

Received: October 21, 2022
Revised: December 12, 2022
Published online: January 12, 2023

[1] J. F. Sherson, H. Krauter, R. K. Olsson, B. Julsgaard, K. Hammerer, I. Cirac, E. S. Polzik, *Nature* **2006**, *443*, 557.
[2] D. S. Sanchez, I. Belopolski, T. A. Cochran, X. Xu, J.-X. Yin, G. Chang, W. Xie, K. Manna, V. Suss, C.-Y. Huang, N. Alidoust, D. Multer, S. S. Zhang, N. Shumiya, X. Wang, G.-Q. Wang, T.-R. Chang, C. Felser, S.-Y. Xu, S. Jia, H. Lin, M. Z. Hasan, *Nature* **2019**, *567*, 500.
[3] X. L. Wang, X. D. Cai, Z. E. Su, M. C. Chen, D. Wu, L. Li, N. L. Liu, C. Y. Lu, J. W. Pan, *Nature* **2015**, *518*, 516.
[4] R. Farshchi, M. Ramsteiner, J. Herfort, A. Tahraoui, H. T. Grahn, *Appl. Phys. Lett.* **2011**, *98*, 162508.
[5] A. B. Kanj, J. Buerck, N. Vankova, C. Li, D. Mutruc, A. Chandresh, S. Hecht, T. Heine, L. Heinke, *J. Am. Chem. Soc.* **2021**, *143*, 7059.
[6] J. R. Brandt, F. Salerno, M. J. Fuchter, *Nat. Rev. Chem.* **2017**, *1*, 0045.
[7] S. C. J. Meskers, *Mater. Adv.* **2022**, *3*, 2324.
[8] X. Shang, L. Wan, L. Wang, F. Gao, H. Li, *J. Mater. Chem. C* **2021**, *10*, 2400.
[9] M. D. Ward, W. Shi, N. Gasparini, J. Nelson, J. Wade, M. J. Fuchter, *J. Mater. Chem.* **2022**, *10*, 10452.
[10] L. Liu, Y. Yang, Z. Wei, *Acta Chim. Sin.* **2022**, *80*, 970.
[11] C. Yan, S. Barlow, Z. Wang, H. Yan, A. K. Y. Jen, S. R. Marder, X. Zhan, *Nat. Rev. Mater.* **2018**, *3*, 18003.
[12] P. Cheng, G. Li, X. Zhan, Y. Yang, *Nat. Photon.* **2018**, *12*, 131.
[13] J. Hou, O. Inganas, R. H. Friend, F. Gao, *Nat. Mater.* **2018**, *17*, 119.
[14] J. D. Servaites, M. A. Ratner, T. J. Marks, *Energy Environ. Sci.* **2011**, *4*, 4410.
[15] L. Zhu, J. Zhang, Y. Guo, C. Yang, Y. Yi, Z. Wei, *Angew. Chem., Int. Ed.* **2021**, *60*, 15348.
[16] F. Lin, K. Jiang, W. Kaminsky, Z. Zhu, A. K. Y. Jen, *J. Am. Chem. Soc.* **2020**, *142*, 15246.
[17] W. Zhu, A. P. Spencer, S. Mukherjee, J. M. Alzola, V. K. Sangwan, S. H. Amsterdam, S. M. Swick, L. O. Jones, M. C. Heiber, A. A. Herzing, G. Li, C. L. Stern, D. M. DeLongchamp, K. L. Kohlstedt, M. C. Hersam, G. C. Schatz, M. R. Wasielewski, L. X. Chen, A. Facchetti, T. J. Marks, *J. Am. Chem. Soc.* **2020**, *142*, 14532.
[18] G. Zhang, X. K. Chen, J. Xiao, P. C. Y. Chow, M. Ren, G. Kupgan, X. Jiao, C. C. S. Chan, X. Du, R. Xia, Z. Chen, J. Yuan, Y. Zhang, S. Zhang, Y. Liu, Y. Zou, H. Yan, K. S. Wong, V. Coropceanu, N. Li, C. J. Brabec, J. L. Bredas, H. L. Yip, Y. Cao, *Nat. Commun.* **2020**, *11*, 3943.
[19] J. Yuan, Y. Zhang, L. Zhou, G. Zhang, H.-L. Yip, T.-K. Lau, X. Lu, C. Zhu, H. Peng, P. A. Johnson, M. Leclerc, Y. Cao, J. Ulanski, Y. Li, Y. Zou, *Joule* **2019**, *3*, 1140.
[20] W. Shi, F. Salerno, M. D. Ward, A. Santana-Bonilla, J. Wade, X. Hou, T. Liu, T. J. S. Dennis, A. J. Campbell, K. E. Jelfs, M. J. Fuchter, *Adv. Mater.* **2021**, *33*, 2004115.
[21] C. Chen, L. Gao, W. Gao, C. Ge, X. Du, Z. Li, Y. Yang, G. Niu, J. Tang, *Nat. Commun.* **2019**, *10*, 1927.
[22] P. Odenthal, W. Talmadge, N. Gundlach, R. Wang, C. Zhang, D. Sun, Z.-G. Yu, Z. V. Vardeny, Y. S. Li, *Nat. Phys.* **2017**, *13*, 894.
[23] G. Long, C. Jiang, R. Sabatini, Z. Yang, M. Wei, L. N. Quan, Q. Liang, A. Rasmita, M. Askerka, G. Walters, X. Gong, J. Xing, X. Wen, R. Quintero-Bermudez, H. Yuan, G. Xing, X. R. Wang, D. Song, O. Voznyy, M. Zhang, S. Hoogland, W. Gao, Q. Xiong, E. H. Sargent, *Nat. Photon.* **2018**, *12*, 528.
[24] V. M. Asnin, A. A. Bakun, A. M. Danishevskii, E. L. Ivchenko, G. E. Pikus, A. A. Rogachev, *Solid State Commun.* **1979**, *30*, 565.
[25] F. de Juan, A. G. Grushin, T. Morimoto, J. E. Moore, *Nat. Commun.* **2017**, *8*, 15995.
[26] G. Chang, B. J. Wieder, F. Schindler, D. S. Sanchez, I. Belopolski, S. M. Huang, B. Singh, D. Wu, T. R. Chang, T. Neupert, S. Y. Xu, H. Lin, M. Z. Hasan, *Nat. Mater.* **2018**, *17*, 978.
[27] D. Rees, K. Manna, B. Z. Lu, T. Morimoto, H. Borrmann, C. Felser, J. E. Moore, D. H. Torchinsky, J. Orenstein, *Sci. Adv.* **2020**, *6*, eaba0509.
[28] X. Shang, I. Song, H. Ohtsu, Y. H. Lee, T. Zhao, T. Kojima, J. H. Jung, M. Kawano, J. H. Oh, *Adv. Mater.* **2017**, *29*, 1605828.
[29] X. Shang, I. Song, J. H. Lee, W. Choi, J. Ahn, H. Ohtsu, J. C. Kim, J. Y. Koo, S. K. Kwak, J. H. Oh, *ACS Nano* **2020**, *14*, 14146.
[30] M. Schulz, F. Balzer, D. Scheunemann, O. Arteaga, A. Luetzen, S. C. J. Meskers, M. Schiek, *Adv. Funct. Mater.* **2019**, *29*, 1900684.
[31] L. Liu, Y. Yang, Y. Wang, M. A. Adil, Y. Zhao, J. Zhang, K. Chen, D. Deng, H. Zhang, K. Amin, Y. Wu, Y. Zhang, Z. Wei, *ACS Mater. Lett.* **2022**, *4*, 401.

[32] L. Zhang, I. Song, J. Ahn, M. Han, M. Linares, M. Surin, H.-J. Zhang, J. H. Oh, J. Lin, *Nat. Commun.* **2021**, *12*, 142.
[33] J. Gilot, R. Abbel, G. Lakhwani, E. W. Meijer, A. P. H. J. Schenning, S. C. J. Meskers, *Adv. Mater.* **2010**, *22*, E131.
[34] Y. Yang, R. C. da Costa, M. J. Fuchter, A. J. Campbell, *Nat. Photon.* **2013**, *7*, 634.
[35] M. D. Ward, J. Wade, X. Shi, J. Nelson, A. J. Campbell, M. J. Fuchter, *Adv. Opt. Mater.* **2022**, *10*, 2101044.
[36] D. Zhu, W. Jiang, Z. Ma, J. Feng, X. Zhan, C. Lu, J. Liu, J. Liu, Y. Hu, D. Wang, Y. S. Zhao, J. Wang, Z. Wang, L. Jiang, *Nat. Commun.* **2022**, *13*, 3454.
[37] A. Wadsworth, Z. Hamid, J. Kosco, N. Gasparini, I. McCulloch, *Adv. Mater.* **2020**, *32*, 2001763.
[38] R. D. Jansen-van Vuuren, A. Armin, A. K. Pandey, P. L. Burn, P. Meredith, *Adv. Mater.* **2016**, *28*, 4766.
[39] L. Liu, Y. Yang, L. Zhu, J. Zhang, K. Chen, Z. Wei, *Small* **2022**, *18*, 2202941.
[40] A. J. Heeger, *Adv. Mater.* **2014**, *26*, 10.
[41] V. D. Mihailetchi, J. Wildeman, P. W. Blom, *Phys. Rev. Lett.* **2005**, *94*, 126602.
[42] K. Ridzonova, E. Belas, R. Grill, J. Pekarek, P. Praus, *Phys. Rev. Appl.* **2020**, *13*, 064054.
[43] B. Jin, H. Park, Y. Liu, L. Liu, J. An, W. Tian, C. Im, *Front Chem. Sci. Eng.* **2020**, *15*, 164.
[44] D. Scheunemann, S. Wilken, O. J. Sandberg, R. Osterbacka, M. Schiek, *Phys. Rev. Appl.* **2019**, *11*, 054090.
[45] I. Hwang, C. R. McNeill, N. C. Greenham, *J. Appl. Phys.* **2009**, *106*, 094506.
[46] C. Labanti, J. Wu, J. Shin, S. Limbu, S. Yun, F. Fang, S. Y. Park, C. J. Heo, Y. Lim, T. Choi, H. J. Kim, H. Hong, B. Choi, K. B. Park, J. R. Durrant, J. S. Kim, *Nat. Commun.* **2022**, *13*, 3745.
[47] A. M. Goodman, A. Rose, *J. Appl. Phys.* **1971**, *42*, 2823.
[48] A. Ligthart, G. H. Gelinck, S. C. J. Meskers, *Org. Electron.* **2016**, *34*, 218.
[49] D. Di Nuzzo, S. van Reenen, R. A. J. Janssen, M. Kemerink, S. C. J. Meskers, *Phys. Rev. B* **2013**, *87*, 085207.